Toxicology and Applied Pharmacology 259 (2012) 54–65

Contents lists available at SciVerse ScienceDirect

Toxicology and Applied Pharmacology

journal homepage: www.elsevier.com/locate/ytaap

Phorate-induced oxidative stress, DNA damage and transcriptional activation of p53 and caspase genes in male Wistar rats

Quaiser Saquib [a], Sabry M. Attia [c], Maqsood A. Siddiqui [a], Mourad A.M. Aboul-Soud [a,f], Abdulaziz A. Al-Khedhairy [a], John P. Giesy [a,d,e], Javed Musarrat [a,b,*]

[a] Department of Zoology, College of Science, King Saud University, Riyadh, Saudi Arabia
[b] Department of Microbiology, Faculty of Agricultural Sciences, AMU, Aligarh, India
[c] Department of Pharmacology, College of Pharmacy, King Saud University, Riyadh, Saudi Arabia
[d] Department of Biomedical and Veterinary Biosciences and Toxicology Centre, University of Saskatchewan, Saskatoon, Canada S7N 5B3
[e] Zoology Department and Center for Integrative Toxicology, Michigan State University, East Lansing 48824, USA
[f] Biochemistry Department, Faculty of Agriculture, Cairo University, 12613 Giza, Egypt

ARTICLE INFO

Article history:
Received 6 June 2011
Revised 4 December 2011
Accepted 5 December 2011
Available online 14 December 2011

Keywords:
Organophosphates
Phorate
Toxicity
Histopathology
Apoptosis
Pesticide

ABSTRACT

Male Wistar rats exposed to a systemic organophosphorus insecticide, phorate [O,O-diethyl S-[(ethylthio) methyl] phosphorothioate] at varying oral doses of 0.046, 0.092 or 0.184 mg phorate/kg bw for 14 days, exhibited substantial oxidative stress, cellular DNA damage and activation of apoptosis-related p53, caspase 3 and 9 genes. The histopathological changes including the pyknotic nuclei, inflammatory leukocyte infiltrations, renal necrosis, and cardiac myofiber degeneration were observed in the liver, kidney and heart tissues. Biochemical analysis of catalase and glutathione revealed significantly lesser activities of antioxidative enzymes and lipid peroxidation in tissues of phorate exposed rats. Furthermore, generation of intracellular reactive oxygen species and reduced mitochondrial membrane potential in bone marrow cells confirmed phorate-induced oxidative stress. Significant DNA damage was measured through comet assay in terms of the Olive tail moment in bone marrow cells of treated animals as compared to control. Cell cycle analysis also demonstrated the G_2/M arrest and appearance of a distinctive SubG_1 peak, which signified induction of apoptosis. Up-regulation of tumor suppressor p53 and caspase 3 and 9 genes, determined by quantitative real-time PCR and enzyme-linked immunosorbent assay, elucidated the activation of intrinsic apoptotic pathways in response to cellular stress. Overall, the results suggest that phorate induces genetic alterations and cellular toxicity, which can adversely affect the normal cellular functioning in rats.

Introduction

Phorate is a systemic and broad spectrum organophosphorus (OP) insecticide, commonly used in agriculture to control sucking and chewing pests. It is also used in pine forests and on root and field crops, including corn, cotton, coffee, and some ornamental plants and bulbs (Abhilash and Singh, 2009; Gan and Jans, 2007). Phorate has been classified as a Class I, high-risk toxic OP compound with an LD_{50} of 1.1 to 3.7 mg/kg bw for rats (http://extoxnet.orst.edu/pips/phorate.htm). It is well known to inhibit acetylcholinesterase activity by phosphorylating the serine hydroxyl group in the substrate binding domain, which results in accumulation of acetylcholine and induces neurotoxicity (Fulton and Key, 2001; Oruc and Usta, 2007; Vandana and Zzaman, 1997). The United States Environmental Protection Agency (USEPA) has authorized restrictions on the use of phorate since 1990 (Devine and Furlong, 2007). However, it is continuously being used in several countries like Italy, China, Egypt and India (Abhilash and Singh, 2009; Mansour et al., 2009; Pagliuca et al., 2006; Wang et al., 2008).

In several epidemiological studies, different OP insecticides have been associated with non-Hodgkin lymphoma (NHL) (Cantor et al., 1992; Zahm et al., 1993), as well as leukemia (Brown et al., 1990; Clavel et al., 1996). Particularly, farming has been significantly associated with prostate cancer (Blair et al., 1985; Bostwick et al., 2004; Checkoway et al., 1987; Mahajan et al., 2006; Sharma-Wagner et al., 2000; Van der Gulden and Vogelzang, 1996; Van Maele-Fabry and Willems, 2004), whereas monozygotic twins have been shown to have a higher prostate cancer concordance than dizygotic twins (Gronberg et al., 1994).

Furthermore, prostate cancer among applicators with a family history of prostate cancer has been linked with exposure to several insecticides including phorate (Alavanja et al., 2003). Phorate has been demonstrated to induce genotoxicity by causing cytogenetic changes, such as sister chromatic exchange (SCE), chromosomal aberrations (CA) and formation of micronuclei (MN) in human lymphoid and Chinese hamster ovary cells (Lin et al., 1987; Sobti et al., 1982). A single intraperitonial dose of 0.75 mg/kg bw of phorate resulted in

* Corresponding author at: Department of Zoology, College of Science, P.O. Box 2455, King Saud University, Riyadh 11451, Saudi Arabia. Fax: +966 4675514.
E-mail address: musarratj1@yahoo.com (J. Musarrat).

0041-008X/$ – see front matter © 2011 Elsevier Inc. All rights reserved.
doi:10.1016/j.taap.2011.12.006

the formation of MN (Grover and Mahli, 1985), while 0.15 or 0.30 mg phorate/kg bw/day for 5 days exhibited greater frequency of CA (Mahli and Grover, 1987) in bone marrow cells of male Wistar rats. Cytogenetic effects of phorate in male Wistar rats including CA and MN were also observed in bone marrow cells of rats exposed to 0.09 to 0.37 or 7.5 to 15 mg phorate/kg bw (Dhingra et al., 1990). In a recent study, Mohanty et al. (2011) reported phorate-induced DNA damage in blood, gill and liver cells of fish (*Labeo rohita*). Comet assay analysis of these cells revealed significant DNA damage in relation to the respective control groups at concentrations of 0.002 or 0.01 ppm. Strong binding of a fungicide with DNA and consequent oxidative DNA damage has been demonstrated previously (Saquib et al., 2010a,b). Such oxidative DNA lesions or adducts might, if not repaired or misrepaired before replication of DNA, eventually result in mutations and initiate carcinogenesis.

Molecular events leading to cyto- and genotoxicity caused by chronic exposure to phorate have not been systematically investigated. Therefore, in this study phorate induced oxidative stress, DNA damage and expression of some apoptotic pathway related genes were assessed in male Wistar rats by use of sensitive molecular assays and techniques. The present study was conducted to determine, if phorate can cause: i) histopathological alterations; ii) cellular oxidative stress, measured in terms of intracellular reactive oxygen species (ROS) generation, changes in oxidative marker enzymes, and mitochondrial membrane potential ($\Delta\Psi m$); iii) DNA strand breaks by the comet assay; iv) cell cycle alterations using flow cytometry; and v) activation of p53, caspase 3 and 9 genes, as indicators of apoptosis in liver of exposed rats.

Methods

Chemicals. Phorate 94.6% pure (CAS No. 298-02-2) was obtained from Agrochemical Division, Indian Agriculture Research Institute (IARI, New Delhi, India). Ethidium bromide (EtBr), propiodium iodide, dimethyl sulfoxide (DMSO), Na_2-EDTA, Tris [hydroxymethyl] aminomethane, RNAse, ethyl methane sulfonate (EMS), 2′,7′-dichlorofluorescin diacetate (DCFH-DA), Rhodamine 123 (Rh123), normal melting (NMA) and low melting point agarose (LMA), RPMI 1640 were purchased from Sigma Chemical Company, St. Louis, MO, USA. Phosphate buffered saline (PBS, Ca^{2+}, Mg^{2+} free), L-glutamine, antibiotic–antimycotic solution was obtained from Hi-Media Pvt. Ltd. (India). Fetal bovine serum (FBS) was procured from BRL Life Technologies Inc. (Gaithersburg, MD, USA). Kits for biochemical analysis of catalase (CAT) (Catalog # 707002), glutathione (GSH) (Catalog # 703002) and lipid peroxidation (LPO) (Catalog # 705002) were purchased from Cayman Chemicals, MI, USA. Enzyme-linked immunosorbent assay (ELISA) based kits for caspase 3/CPP32 (catalog #K106-25) and caspase 9 colorimetric assay (catalog #K119-25) were purchased from Biovision, CA USA. One third frosted slides (76×26×1 mm) and micro cover glasses (24×60 mm) for comet assay were obtained from Marienfeld, Germany. All other chemicals were of analytical grade.

Animals, diet and housing. Adult male Wistar rats 8–9 weeks old, weighing 150±10 g were obtained from the experimental animal care center, College of Pharmacy, King Saud University, Riyadh, SA. Rats were maintained under standard conditions of humidity, temperature (25±2 °C) and light (12-h light/12-h dark). Animals were given standard pellet diet and water ad libitum. Experiments were conducted according to the guidelines of the animal care and use committee at the College of Science, King Saud University, Riyadh.

Treatment of rats. Prior to exposure, rats were acclimatized for one week and then randomly divided into five groups of five individuals. Rats were exposed via oral gavage. Group I was the vehicle control and received DMSO (0.8%) in corn oil. Groups II, III and IV were given 0.046, 0.092 or 0.184 mg phorate/kg bw/day up to 14 days. These doses represented 1/80th, 1/40th and 1/20th of the LD_{50}, of 1.1–3.7 mg phorate/kg bw/day, respectively (http://extoxnet.orst.edu/pips/phorate.htm). The greatest LD_{50} value of 3.7 mg/kg was used as a reference for calculating the 1/80th, 1/40th and 1/20th divisors for treatment doses. Group V was a positive control for the comet assay and was given 100 mg EMS/kg bw in corn oil 24 h before being killed. At the termination of experiments all animals were killed while anesthetized.

Histopathology. Qualitative changes in tissues were determined histologically in liver, kidney and heart. In brief, the tissues were sliced into 5–6 mm thick sections and fixed for 48 h in10% formaline, dehydrated in an ascending graded series of ethanol, cleared in toluene and embedded in paraffin. Sections of the tissues were cut by rotary microtome and stained with hematoxylin and eosin for microscopic observations. The remaining portions of organs were snap frozen in liquid N_2 and kept at −80 °C for quantitative real-time PCR (qPCR) and biochemical analysis.

Biochemical assays.

a) *Catalase activity*. Catalase activity in liver tissues was measured using a catalase assay kit, following the manufacturer's protocol. In brief, liver (1 g) was homogenized in 5 ml cold buffer (50 mM potassium phosphate; 1 mM EDTA, pH 7.0) and centrifuged at 16,060×*g* for 15 min at 4 °C. The supernatant was aspirated and collected for performing the assay. A reaction mixture was prepared by adding 100 µl of assay buffer, 30 µl of methanol and 20 µl of tissue supernatant sample in sterile 96-well plate. The reaction was initiated by adding 20 µl of hydrogen peroxide and incubated on a shaker for 20 min at room temperature. The reaction was stopped by addition of 30 µl of potassium hydroxide. Subsequently, chromogen (30 µl) was added and incubated at room temperature for 10 min followed by addition of potassium periodate (10 µl). The microtiter plate was then kept on a shaker at room temperature for 5 min and the absorbance was read at 540 nm using Multiwell Microplate Reader (Biochrom Anthos Zenyth 200, Cambridge, UK).
b) *Total glutathione (GSH)*. Concentration of GSH in liver was measured by use of commercially available kit as per manufacturer's instructions. In brief, liver (1 g) was homogenized in 5 ml of cold MES buffer (Cayman Chemicals, MI, USA). The homogenate was centrifuged at 16,060×*g* for 15 min at 4 °C. Supernatant was collected and deproteinated for the assay. Freshly prepared assay cocktail (150 µl) was added to 50 µl of the deproteinated sample in 96-well plate and the absorbance was read after 25 min at 405 nm using microplate reader.
c) *Lipid peroxidation (LPO)*. LPO in liver was estimated by use of commercially available kit following manufacturer's protocol. In brief, liver (1 g) was homogenized in HPLC-grade water and lipid hydroperoxides were extracted into chloroform before performing the assay. The chloroform-ethanol mixture (450 µl) was added to the chloroform extract (500 µl) of each sample. Freshly prepared chromogen (50 µl) was then added to each assay tube and mixed. The tubes were kept at room temperature for 5 min. Final suspensions (300 µl each) were then transferred to 96-well plates and read at 500 nm using the microplate reader.

Isolation of bone marrow cells. Bone marrow cells were isolated following a previously published method (Sushila et al., 2006). In brief, both rat femurs were taken out by dissection and cleaned to remove muscles and other tissues. Bone marrow cells were flushed in 1.5 ml FBS using a syringe and centrifuged at 1200×*g* for 4 min. Cell pellets were washed twice with 1 ml of PBS to remove FBS. Cells were then re-suspended in 2 ml PBS (Ca^{2+} and Mg^{2+} free). Aliquots of 500 µl of cell suspension were prepared in four separate tubes for quick processing of cells for the comet assay, flow cytometric analysis of cell cycle progression, intracellular ROS generation and $\Delta\Psi m$. The

number of cells was adjusted to ~1.0×10^6 cells/ml for all the parameters studied. Trypan blue was used to determine viability of cells isolated from bone marrow.

Comet assay. The comet assay was performed in bone marrow cells, according to the in vivo comet assay guidelines of Tice et al. (2000), as described by Saquib et al. (2009). In brief, 100 μl bone marrow cell suspension of vehicle (negative control), EMS-treated (positive control), and phorate-treated rats were mixed with 100 μl of 1% LMA. The cell suspension (80 μl) was then layered onto one-third frosted slides, pre-coated with NMA (1% in PBS) and kept at 4 °C for 10 min. After gelling, a layer of 90 μl of LMA (0.5% in PBS) was added. Cells were lysed overnight in a lysing solution. After washing with Milli Q water, slides were subjected to DNA denaturation in cold electrophoretic buffer at 4 °C for 20 min. Electrophoresis was performed at 0.7 V/cm for 30 min (300 mA, 24 V) at 4 °C. Slides were then washed three times with neutralization buffer. To prevent secondary DNA damage, preparative steps were conducted in darkness. Each slide was stained with 75 μl of 20 μg/ml ethidium bromide solution for 5 min. Slides were analyzed at 40× magnification (excitation wavelength of 515–560 nm and emission wavelength of 590 nm) by use of a fluorescence microscope (Nikon Eclipse 80i, Japan), which was coupled with a charge coupled device (CCD) camera. Images from 100 cells (50 from each replicate slide) were randomly selected and subjected to image analysis with software Comet Assay IV (Perceptive Instruments, Suffolk, UK). Mean values of the Olive tail moment (OTM), tail length (μm) and tail intensity (%) were separately analyzed for statistical significance. The level of statistical significance chosen was $p \leq 0.05$, unless otherwise stated.

Estimation of ROS generation. In vivo intracellular ROS production was detected using the fluorescent probe DCFH-DA, following the method described by Bakheet et al. (2011). In brief, bone marrow cells (500 μl) were incubated in the dark with DCFH-DA (5 μM) for 60 min at 37 °C. Cells were immediately washed twice with PBS at 3600×*g* for 5 min at room temperature and pellets were re-suspended in 500 μl PBS. The fluorescence of cells was recorded under 488 nm excitation. Green fluorescence from DCF was measured in the FL1 Log channel through a 525 nm band-pass filter by a Beckman Coulter flow cytometer (Coulter Epics XL/Xl-MCL, USA). Data were presented as the mean fluorescence (MnXI) of 10,000 cells.

Phorate-induced intracellular ROS generation was also determined in vitro, according to methods described by Saquib et al. (2009). Briefly, rat bone marrow cells (1×10^6 cells/ml) from untreated rats were isolated and treated with varying concentrations (5, 10, 25, 50, 100, 250 or 500 μM) of phorate in complete RPMI 1640 medium for 1 to 4 h at 37 °C in a CO_2 incubator (Heracell 150i, Thermo Scientific, Finland). After incubation, cells were pelleted by centrifugation at 3600×*g* for 5 min, and washed twice with cold PBS, and again re-suspended in 500 μl of PBS. Cells were then incubated in the dark with DCFH-DA (5 μM) for 60 min at 37 °C. Cells were immediately washed twice with PBS and finally suspended in 500 μl PBS. The fluorescence intensity of DCF was measured by use of a microplate fluorometer (Thermo Scientific Fluoroskan Ascent, Finland) at an excitation wavelength of 485 nm and emission wavelength of 538 nm. The percent change in DCF fluorescence was determined by considering the fluorescence intensity of untreated control cells as 100%.

Measurement of $\Delta\Psi m$. Flow cytometric measurements of $\Delta\Psi m$ were performed following the method described by Bakheet et al. (2011). In brief, bone marrow cells (500 μl) were incubated with mitochondrial-specific fluorescence dye Rh123 (5 μg/ml) for 60 min at 37 °C in dark with gentle shaking. Cells were immediately washed twice with PBS at 3600×*g* for 5 min at room temperature and pellets were re-suspended in 500 μl PBS. $\Delta\Psi m$ was measured by use of flow cytometry and expressed as the mean fluorescence intensity (MnXI) of 10,000 cells.

Cell cycle analysis. Bone marrow cells (500 μl) were fixed with ice-cold 70% ethanol, and incubated at 4 °C for 1 h. After two washes with PBS, cells were centrifuged at 3600×*g* for 5 min. Then cell pellets were re-suspended in PBS and stained with propiodium iodide (50 μg/ml) containing 0.1% Triton X-100 and 0.5 mg/ml RNAase A for 1 h at 30 °C in the dark. Red fluorescence intensities of 10,000 cells stained with propiodium iodide were acquired in FL4 Log channel through a 675 nm band-pass filter (Bakheet et al., 2011; Darzynkiewicz et al., 1992) by use of a Beckman Coulter flow cytometer. DNA content was determined by Coulter Epics XL/XL-MCL, System II Software, Version 3.0. Cell debris, characterized by low FSC/SSC was excluded from the analysis.

Isolation of total RNA and real-time PCR (qPCR). Total RNA was purified from 10 mg of rat liver using the iPrep™ PureLink™ kit (Invitrogen, USA) by an Invitrogen® automated system following the manufacturer's protocol. Purity of total RNA was measured by use of a Nanodrop 8000 spectrophotometer (Thermo Scientific, USA) and the integrity of RNA was visualized on 1% agarose gel by use of a gel documentation system (Universal Hood II, BioRad, USA). RNA was stored at −80 °C until processed for cDNA synthesis. The first-strand cDNA synthesis was performed with 1 μg of total RNA and 100 ng of oligo-p$(dT)_{12-18}$ primer and MLV Reverse Transcriptase (GE Health Care, UK) according to the manufacturer's recommendations. The following sets of specific primers were employed for amplification of each cDNA: p53 (5′ F-GT-CGGCTCCGACTATACCACTATC-3′, 5′R-CTCTCTTTGCACTCCCTGGGGG-3′), caspase 3 (5′F-CAGAGCTGGACTGCGGTATTGA-3′,5′R-AGCATGGCGC-AAAGTGACTG-3′), caspase 9 (5′F-AGCCAGATGCTGTCCCATAC-3′, 5′R-CAGGAGACAAAACCT GGGAA-3′) and GAPDH (5′F-GCTGCCTTCTCT-TGTGACAAAGT-3′, 5′-CTCAGCCTTGACTGTGCCATT-3)′. Expression was normalized to GAPDH gene expression, which was used as an internal housekeeping control. Real-time quantification was performed in the LightCycler® 480 instrument with 96-well plate (Roche Diagnostics, Rotkreuz, Switzerland) using the qPCR GreenMaster based on EvaGreen fluorescent DNA stain (Jena Bioscience GmbH, Germany). PCR mixtures (final volume of 10 μl) contained 5 μl of qPCR GreenMaster, 2 μl of a 10^{-1} dilution of the cDNA and 300 nM of each primer. Cycling conditions included an initial heat-denaturing step at 95 °C (Ramp Rate 4.4 C°/s) for 5 min, 50 cycles at 95 °C for 20 s (Ramp Rate 4.4 C°/s), annealing at 60 °C for all the primers for 15 s (Ramp Rate 2.2 C°/s), and product elongation and signal acquisition (single mode) at 72 °C for 15 s (Ramp Rate 4.4 C°/s). Following amplification, the melting curves were determined in a three-segment cycle of 95 °C for 0 s, 65 °C for 15 s, and 95 °C for 0 s at the continuous acquisition mode. The temperature transition rates were set at 20 °C/s except for segment three of the melting curve analysis, where it was set to 0.1 °C/s. Water was used as the template for negative control amplifications included with each PCR run. Serial dilutions of each cDNA (10^{-1}–10^{-6}) were used to generate a quantitative PCR standard curve to calculate the corresponding PCR efficiencies. Results were obtained from three subsamples and PCR was repeated twice per sample. Relative quantification analysis was performed by use of a Roche LightCycler® 480 software Version 3.5. Expression of mRNA normalized to the GAPDH gene was calculated, and the data were subjected to *t*-test in order to identify significant differences between animals treated with phorate compared to untreated control.

Caspases 3 and 9 activities. In order to investigate the involvement of caspases 3 and 9 in signaling transduction, cleavage products of caspases 3 and 9 were detected by ELISA using the caspase 3 and caspase 9 colorimetric assay kits, following the protocol described by the manufacturer. In brief, liver (100 mg) was homogenized in 500 μl of chilled lysis buffer and incubated on ice for 60 min. Insoluble proteins and nuclei were removed by centrifugation at 14,800×*g* and 4 °C for 10 min. The supernatant was used to estimate the caspase 3 and 9 activities. Protein in supernatant was quantitated by the method of Lowry et al. (1951) with bovine serum albumin as standard. The

equivalent of 200 μg of protein from the supernatant was diluted to 50 μl with cell lysis buffer. To this, 50 μl of 2× reaction buffer (containing 10 mM dithiothreitol) and 5 μl of the 4 mM DEVD-pNA caspase 3 substrate or 4 mM LEHD-pNA caspase 9 substrate (200 μM final concentration of each) were added. After 2 h incubation at 37 °C, formation of p-nitroanilide was measured at 405 nm by use of a microplate reader (Multiskan Ex, Thermo Scientific, Finland).

Statistical analysis. Individual rats were the experimental unit. Data were expressed as mean ± SD for the values obtained from at least three independent experiments. Statistical analyses were performed by one-way analysis of variance (ANOVA) followed by Dunnett's multiple comparison test (Sigma Plot 11.0, USA). The level of statistical significance chosen was $p<0.05$, unless otherwise stated.

Results

Histology of liver, kidney and heart

Histopathological analysis of liver, kidney and heart tissue sections of rats exposed to phorate showed abnormalities as compared to the control rats. Liver of unexposed rats exhibited normal polyhedral hepatocytes and the boundaries of the sinusoids exhibited a single layer of fenestrated endothelial cells and Kupffer cells (Fig. 1, panels A and B). However, hepatocytes of rats exposed to the greatest concentration (0.184 mg/kg bw/day) of phorate were damaged. The hepatocytes were characterized by the appearance of pyknotic nuclei, fatty infiltrations, inflammatory leukocyte infiltrations and activated Kupffer cells, dilatation in blood sinusoids and extensive cytoplasmic vacuolization (Fig. 1, panels C–F). Kidney of control rats exhibited a normal renal cortex with proximal and distal convoluted tubules surrounding renal corpuscles with normal Bowman's space and blood vessel (Fig. 2, panels A, B). In contrast, kidney of rats exposed to phorate exhibited a greater Bowman's space with infiltration of renal parenchyma by inflammatory leukocytes, dilated blood vessels and renal necrosis of the cells (Fig. 2, panels C–F). Heart also exhibited congestion and hemorrhage, cardiac myofiber degeneration and round and shrunken focal degenerating myocytes in rats exposed to phorate (Fig. 3, panels B and C), relative to the normal longitudinally striated myocytes in control heart tissue (Fig. 3, panel A).

CAT activity, GSH and LPO levels

Significant differences in catalase activity, GSH, and LPO levels were observed in liver of rats exposed to phorate. Less (21.9 and 37.3%, $p \leq 0.05$) catalase activity in phorate treated rats were observed at the highest doses of 0.092 and 0.184 mg/kg bw/day, respectively as compared to untreated controls (Fig. 4, panel A). Further,

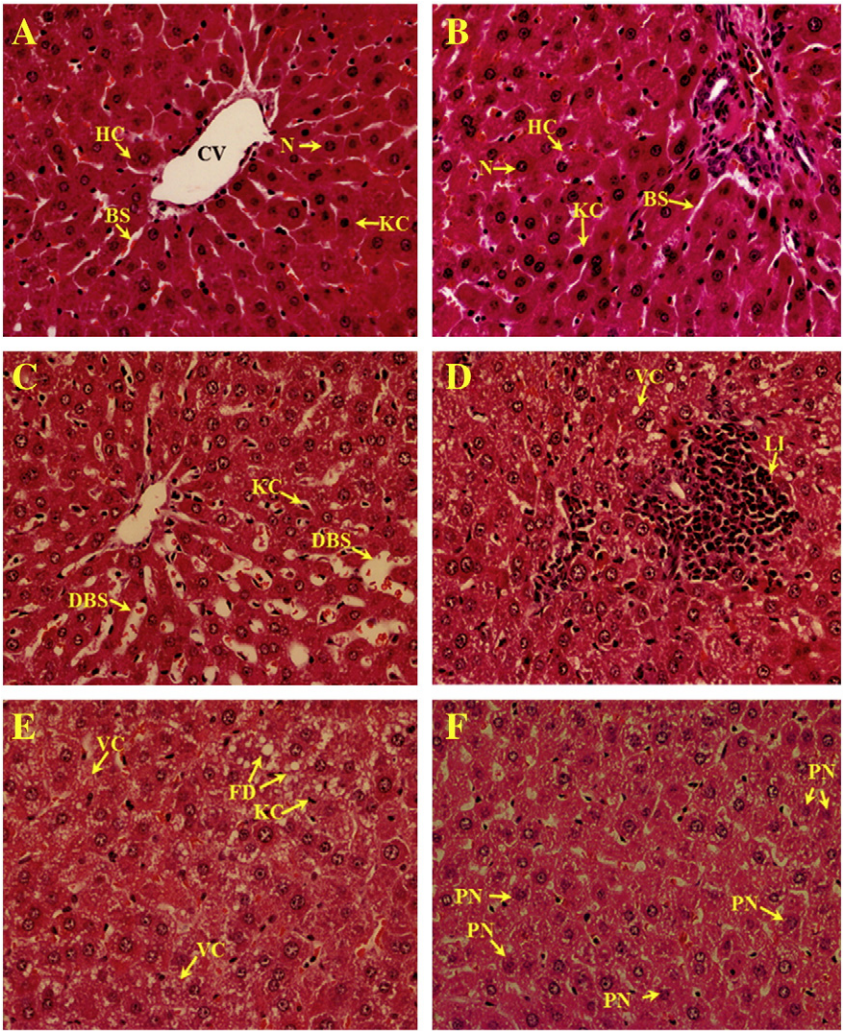

Fig. 1. Phorate-induced histopathological abnormalities in rat liver (×400). Panels A and B: liver sections of control animals showing normal histological appearance of the liver, including central vein (CV), blood sinusoids (BS), hepatic cells (HC), Kupffer cell (KC) and centrally located nuclei (N). Panels C–F: liver sections of phorate treated animals exhibiting appearance of pyknotic nuclei (PN), fatty infiltrations (FD), inflammatory leukocyte infiltrations (LI) and activated Kupffer cells (KC), dilatation in blood sinusoids (DBS) and cytoplasmic vacuoles (VC). Each photomicrograph represents a section from an individual liver.

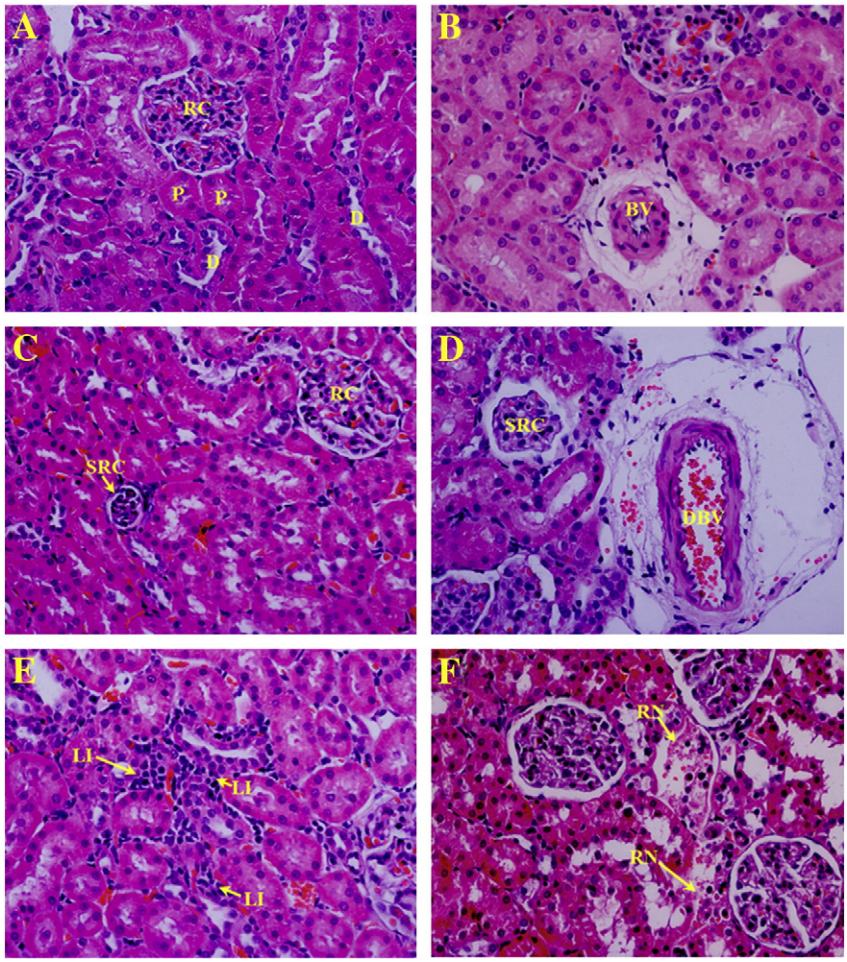

Fig. 2. Phorate-induced histopathological abnormalities in rat kidney (×400). Panels A and B: kidney sections of control animals showing normal histological appearance of renal cortex (RC), proximal (P), distal (D) and normal blood vessels (BV). Panels C–F: kidney sections of phorate treated animals exhibiting the appearance of shrinked renal cortex (SRC), dilated blood vessel (DBV), inflammatory leukocyte infiltrations (LI) and renal necrosis (RN). Each photomicrograph represents a section from an individual kidney.

significantly lesser (25.5 and 31.5%, $p \leq 0.05$) GSH (Fig. 4, panel B), and greater (28.3% and 54.7%, $p \leq 0.05$) LPO were also observed in rats exposed to 0.092 or 0.184 mg/kg bw/day, respectively, as compared to controls (Fig. 4, panel C).

DNA damage in bone marrow

Significantly greater DNA damage in bone marrow cells was observed in rats exposed to phorate, by use of the comet assay. The OTM values at 0.092 or 0.184 mg/kg bw/day phorate were 6.1 ± 0.22 and 9.4 ± 0.13 ($p<0.05$), respectively, compared to 0.6 ± 0.09 in controls. Thus, exposure to the greatest concentration of phorate resulted in 14.6-fold greater DNA damage than the vehicle control (Table 1). More than 90% of cells from vehicle controls had comet tail lengths in the range of 10 to 20 μm. However, 40% and 55% of cells exhibited the DNA comet tail lengths of 30 to 65 and 30 to 90 μm in cells of rats treated to phorate at 0.092 or 0.184 mg/kg bw/day, respectively (Supplementary Fig. 1).

In vivo and in vitro ROS generation in rat bone marrow cells

Significantly greater intracellular generation of ROS was observed in treated bone marrow cells in vivo exposed to phorate. Compared to the DCF fluorescence (MnXI) of vehicle controls, ROS generation was determined to be 1.1, 1.4 and 1.6-fold ($p<0.05$) at phorate doses of 0.046, 0.092 or 0.184 mg/kg bw/day, respectively (Fig. 5, panels I and II). In order to ascertain the potential of phorate for inducing oxidative stress during the initial hours of treatment, ROS generation under in vitro conditions was determined. Supplementary Fig. 2 shows the enhancement of DCF fluorescence in phorate post-treated rat bone marrow cells. The concentration-dependent greater DCF fluorescence intensities were invariably observed at all post-treatment time points. Significant ($p<0.01$) time dependent greater fluorescence intensity of DCF was observed as 25.6%, 22.4%, 24.8% and 34.1% after 1, 2, 3, or 4 h of treatment, respectively at the greatest concentration of 500 μM phorate.

Mitochondrial membrane potential ($\Delta\Psi m$)

Phorate-induced differences in the $\Delta\Psi m$ in phorate treated animals were recorded in terms of fluorescence intensity of mitochondria specific dye rhodamine (Rh 123). A concentration-dependent decrease in Rh 123 fluorescent intensity was observed in rats treated with phorate (Fig. 6, panels I and II). Based on flow cytometry analysis, the extent of reduction in $\Delta\Psi m$, due to exposure to phorate was 1.8-fold at 0.184 mg/kg bw/day, relative to the untreated control.

Cell cycle progression

G_2/M cell cycle arrest was evident from the appearance of 34.0 and 44.4% of bone marrow cells in G_2/M phase in rats treated with 0.046 and 0.092 mg phorate/kg bw, respectively vs. 20.0% of cells in G_2/M phase in the vehicle control. The greatest dose of 0.184 mg phorate/

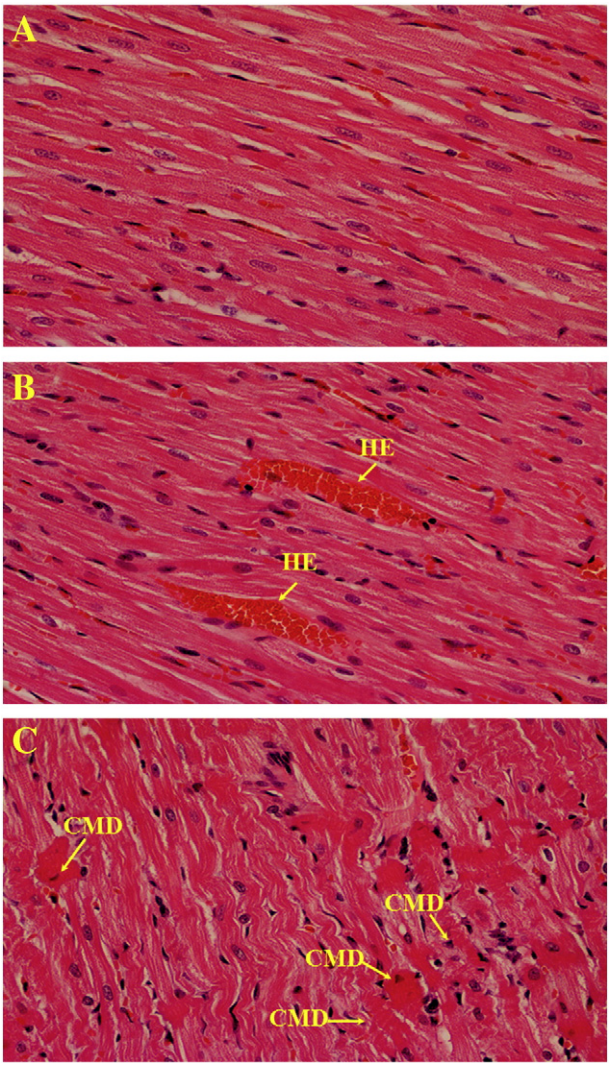

Fig. 3. Phorate-induced histopathological abnormalities in rat heart (×400). Panels are represented as, (A): heart sections of control animals showing the normal cardiac myofibers; (B): heart sections of phorate treated animals showing congestion and hemorrhage (HE); (C): cardiac myofiber degeneration (CMD) in phorate treated animals, focal degenerating myocytes are round and shrunken compared to the normal myocytes that are longitudinally striated. Each photomicrograph represents a section from an individual heart.

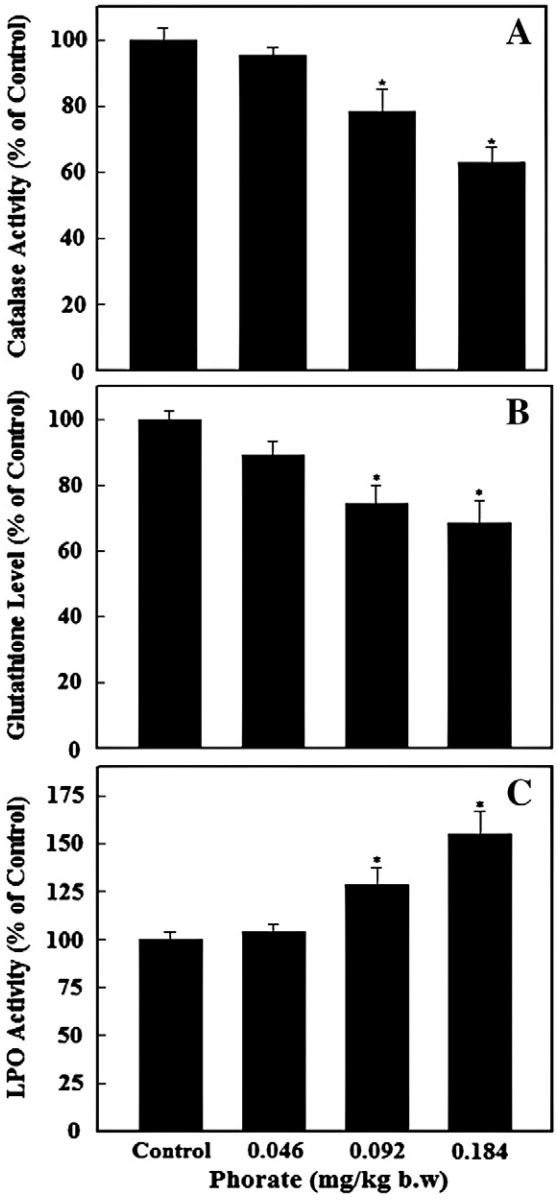

Fig. 4. Effect of phorate treatment on catalase activity (panel A), glutathione level (panel B) and lipid peroxidation activity (panel C) in rat liver tissue after 14 day exposure. Values are expressed as mean ± S.D. of five animals in each group. (*) represents significant difference from control ($p<0.05$).

kg bw/day caused an apoptotic response, which was characterized by appearance of a distinctive $SubG_1$ peak (38.5%) vs. the vehicle control group, which exhibited only 7.0% of cells in the $SubG_1$ (Fig. 7, panels I and II).

Differential expression of p53, caspase 3 and 9 genes

Expression of tumor suppressor (p53), caspase 3 and 9 genes in liver of rats exposed to phorate for 14 days were significantly up-regulated. Relative to the solvent control a significant 264, 172.4 and 317% up-regulation in the mRNA expression of p53 gene was observed in livers of rats treated with 0.046, 0.092 or 0.184 mg/kg bw/day, respectively (Fig. 8). Up-regulation of mRNA expression of the caspase 3 and 9 genes was also observed in rats treated with phorate. Up-regulation of mRNA expression of the caspase 3 and 9 genes in rats exposed to 0.046, 0.092 or 0.184 mg phorate/kg bw/day were 220.7, 302.4, 167.5 and 286, 313, 223.2%, respectively which were significantly ($p<0.05$) greater than that of the vehicle controls.

Effect of phorate treatment on caspase 3 and 9 activities

Since, activation of caspases plays a critical role in apoptosis and signal transduction, activities of caspases 3 and 9 were measured by ELISA. The results in Fig. 9 (panels A and B) showed 1.2 and 1.6-fold ($p<0.05$) greater caspase 3 activity in liver tissue of rats treated with 0.092 or 0.184 mg/kg bw/day, respectively, of phorate. Similarly, the activity of caspase 9 toward LEHD-pNA was 2.7 and 3.6-fold greater ($p<0.05$) at the same doses of phorate as compared with the untreated control.

Discussion

Until now, most of the information on toxicity of phorate was available in the form of unpublished studies conducted by chemical companies solely for registration or marketing purposes. These studies presented information on conventional assays and did not provide

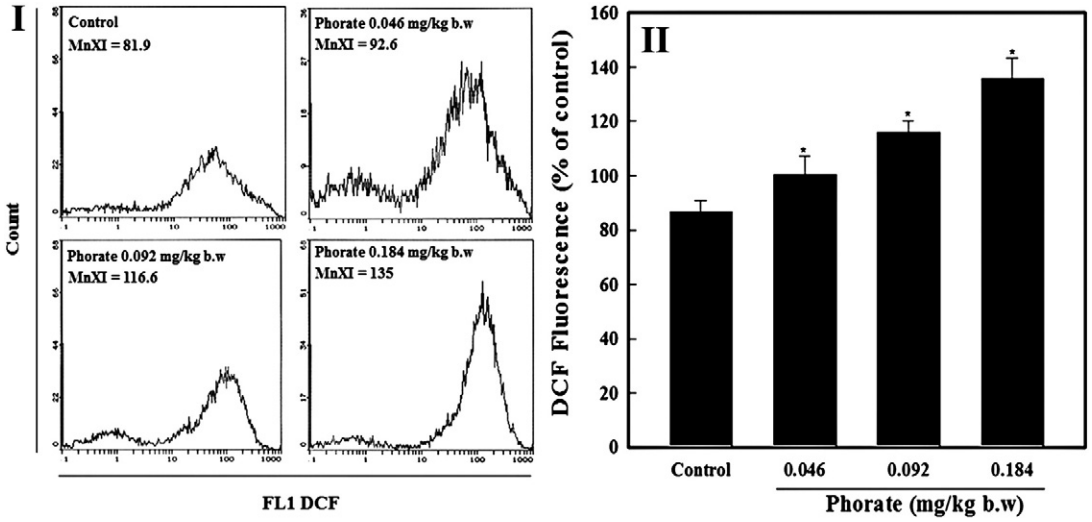

Fig. 5. Intracellular ROS generation in bone marrow cells of phorate treated rats. Panel I is a representative FACS image from a single animal exhibiting an increase in the DCF fluorescence as a function of phorate concentration. Each histogram in panel II represents mean ± S.D. values of DCF fluorescence obtained from all animals (n = 5) treated with varying concentrations of phorate. (*) represents significant difference from control ($p<0.05$) using one-way ANOVA (Dunnett multiple comparison test). Control: represents the solvent control (DMSO 0.8%); MnXI: represents the mean value of DCF fluorescence obtained from 10,000 bone marrow cells.

quantitative assessments of damage to genetic material or other information on mechanisms of action. The general lack of information on the nature of phorate toxicity and molecular events involved in the in vivo toxicity during more chronic exposures (2 weeks) at lesser doses prompted us to conduct in vivo studies. Unlike some other insecticides, the data on molecular dosimetry, residual environmental toxicity and accidental or professional exposures to phorate are limited. Also, there are conflicting reports on the in vitro and in vivo cytogenicity effects of phorate (http://www.gezondheidsraad.nl/en/publications/health-based-reassessment-administrative-occupational-exposure-limits-phorate). In most of the studies, the doses of phorate used were greater than those selected for this study. Ivett and Myhr (1986) exposed rats to 2.5 mg/kg/day through intraperitonial injection with durations of exposure varying from 24 h (Pandita, 1986) to 5 days (Grover and Mahli, 1985; Mahli and Grover, 1987). Doses of 0.15 to 0.30 mg phorate/kg bw/day and 7.5 to 15 mg phorate/kg bw have been shown to induce greater frequency of CA and MN in rat bone marrow cells (Dhingra et al., 1990; Mahli and Grover, 1987). The threshold of detection of cellular and genetic damage depends on sensitivity of assays, experimental conditions and model systems used. Thus, in this study, doses of 0.046, 0.092 or 0.184 mg phorate/kg bw/day were administered orally for 14 days. The selected doses appear small compared to a single intraperitonial dose of 0.75 mg/kg bw of phorate, that causes MN formation in bone marrow cells of male Wistar rats (Grover and Mahli, 1985). Recently, Mohanty et al. (2011) detected DNA damage in fish cells by comet assay at several fold lesser concentrations (0.002 or 0.01 μg/ml) than the doses used in this study. Our comet data on rat bone marrow cells revealed significant DNA damage at relatively greater doses of 0.092 or 0.184 mg phorate/kg bw/day. Unfortunately, there is no other data for the same model system to which

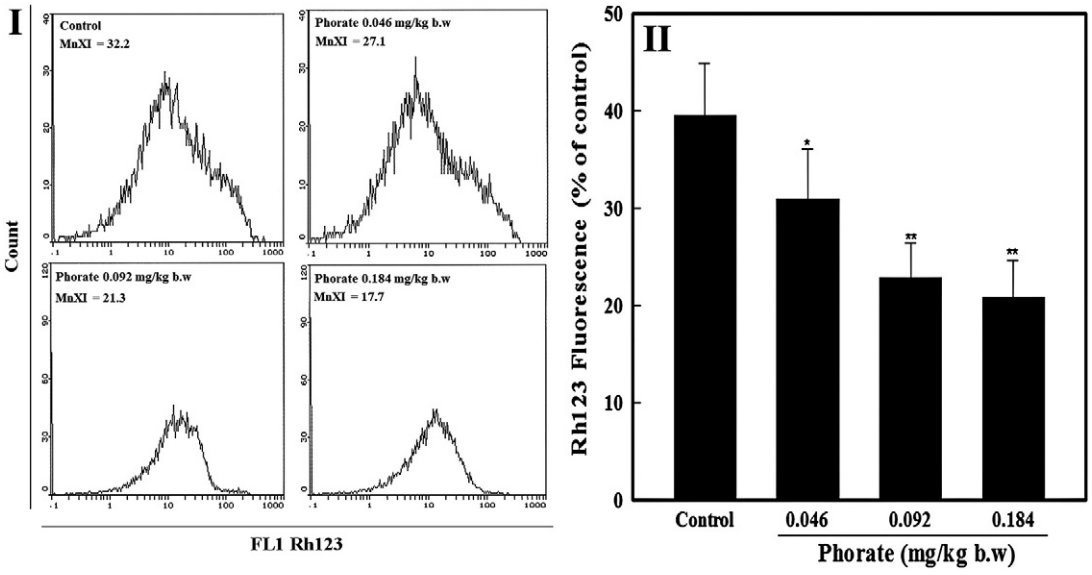

Fig. 6. Assessment of mitochondrial membrane potential in bone marrow cells of phorate treated rats. The fluorescence of Rh123 was measured using a flow cytometer on log scale with FL1 filter. Panel I is a representative FACS image from a single animal exhibiting decline in the Rh123 fluorescence as a function of phorate concentration. Each histogram in panel II represents mean ± S.D. values of Rh123 fluorescence obtained from all animals (n = 5) treated with varying concentrations of phorate. *$p<0.05$, ** $p<0.01$ as compared to control using one-way ANOVA (Dunnett multiple comparison test). Control: represents the solvent control (DMSO 0.8%); MnXI: represents the mean value of Rh123 fluorescence obtained from 10,000 bone marrow cells.

Table 1
Dose dependent change in the DNA damage parameters of comet assay in bone marrow cells of rats exposed to varying concentrations of phorate for 14 days.

Groups	Olive tail moment (arbitrary unit)	Tail length (μm)	Tail intensity (%)
Group I	0.6 ± 0.09	24.1 ± 1.16	6.6 ± 1.00
Group II	0.9 ± 0.14	27.1 ± 1.16	9.3 ± 1.00
Group III	6.1 ± 0.22*	35.6 ± 2.98*	19.9 ± 0.96*
Group IV	9.4 ± 0.13*	46.7 ± 1.72*	26.8 ± 0.49*
Group V	18.5 ± 2.41*	77.6 ± 3.34*	59.2 ± 3.96*

Data are the mean ± S.E.M of 100 cells/animal (50 cells from each slide) of five animals in each group. Statistical significance were determined by one way ANOVA using Dunnett's test at * $p<0.05$. Group I; vehicle control, groups II–IV; phorate 0.046, 0.092 and 0.184 and mg/kg b.w., group V; EMS 100 mg/kg b.w.

to compare. Nevertheless, the doses used in this study have a scientific rationale and also the significant biochemical and genetic changes measured have validated the potency of selected treatment doses, which may help in redefining the phorate exposure doses for human health risk assessment.

OP pesticides, such as phorate, have been reported to induce various degenerative changes including vacuolation and necrosis of liver (Gupta et al., 1981; Hassan et al., 1991; Numan et al., 1990). In this study, histological investigations of tissues demonstrated changes in liver in all treated groups. The abnormal histology observed in liver, which included the presence of pyknotic nuclei (necrosis), fatty and inflammatory were consistent with phorate-induced cellular injury. The observed changes including leukocyte infiltrations, activated Kupffer cells, dilatation in blood sinusoids and extensive cytoplasmic vacuolization were in agreement with the results of Morowati (1997), who also reported hepatocellular necro-inflammation, mild to severe multifocal cloudy, hydropic and fatty degenerations and necrosis in liver sections of phorate-treated, male, Swiss albino mouse (*Mus musculus*). Similar histological alterations, including greater vacuolization, hepatocyte necrosis and dilatation of sinusoids in rat liver exposed to chlorpyrifos and 2,4-D have been reported (Goel et al., 2005; Tayeb et al., 2010).

Kidney function such as renal blood flow, concentrating substances, and biotransformation of the parent compounds makes this tissue sensitive to a variety of toxins. Although, activities of metabolizing enzymes in kidney are less than those in liver, but the enzymatic reactions occurring in the liver have also been shown in the kidney. The greater Bowman's space with infiltration of renal parenchyma by inflammatory leukocytes, dilated blood vessels and renal necrosis in sections of kidney from treated animals observed in this study was similar to the results of Morowati (2001), who has also reported that inhalation of phorate resulted in impairment of glomerular function and tubular damage with mild to severe multifocal cloudy and hydropic degeneration (edema) with necrosis in kidney tubules of mice.

The shrunken and hypereosinophilic myocytes, pyknotic nuclei (necrosis) and myofiber degeneration observed in heart in this study were similar to changes reported previously by Britt et al. (2000) in *Rhesus macaques* exposed to soman, an OP insecticide, for ten days. Those authors reported lesions in heart including myocardial degeneration and necrosis. The observed infiltration of leucocytes and the presence of necrotic cells have been reported as indicators of oxidative stress (Glende et al., 1976; Hassan et al., 1991). Oxidative stress could lead to further damage to cell membranes and proteins, including enzymes, which eventually results in loss of membrane fluidity and function.

Substantial phorate-induced generation of intracellular ROS is attributed to mitochondrial dysfunction and lesser activities of the antioxidant enzymes CAT, GSH and greater LPO, were observed in liver of rats exposed to phorate. Our data on in vitro ROS measurement in phorate treated bone marrow cells suggested early-stage ROS generation. Greater generation of ROS and lesser activities of CAT and GSH signify failure of the antioxidant defense systems responsible to overcome the influx of ROS. It is known that the oxidative stress occurs as a consequence of imbalance between the production of ROS and antioxidative process in favor of free radical production (Dringen, 2000). Also, earlier studies demonstrated altered cellular redox homeostasis due to OP pesticides induced production of ROS, and depletion or impairment of antioxidant enzymes (Bagchi et al., 1995; Muniz et al., 2008), which is consistent with our results. Moreover, inhibition of enzymes involved in removal of free radicals might result in accumulation of H_2O_2, which has been suggested to promote lipid peroxidation, modulation of DNA, altered gene expression and cell death (Fetoui et al., 2009; Halliwell and Gutteridge, 1999).

Alterations in mitochondrial activity based on cationic fluorescent probe Rh123 observed in this study are further evidence of the role of

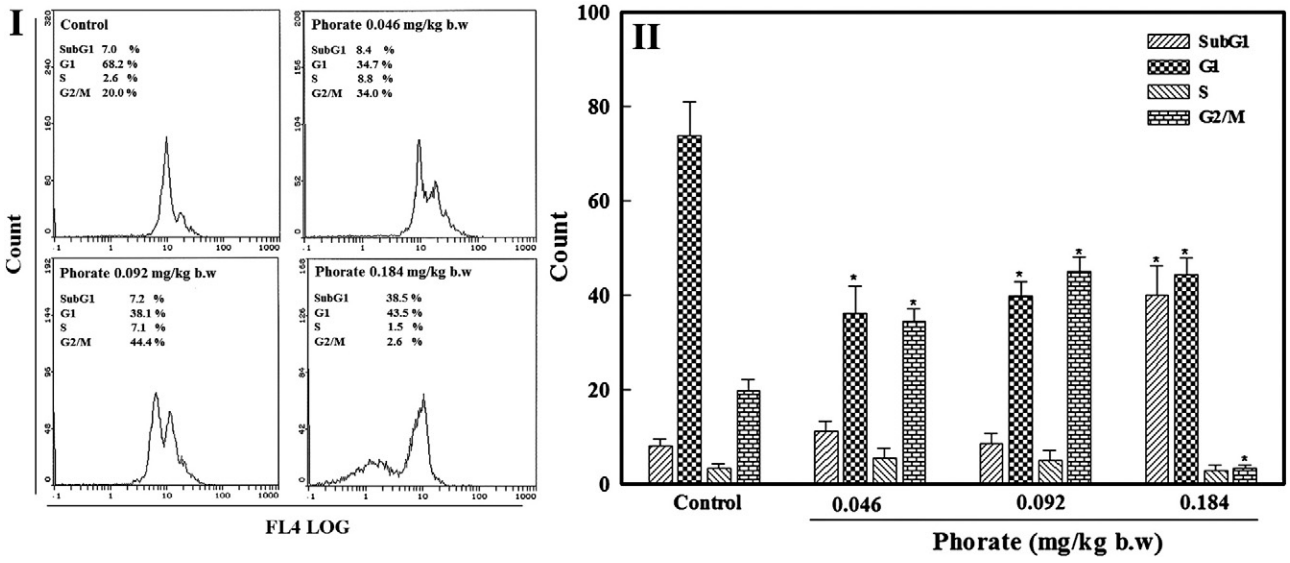

Fig. 7. Cell cycle analysis in bone marrow cells of phorate treated rats. Panel I is a representative FACS image obtained from a single animal exhibiting changes in the progression of normal cell cycle as a function of phorate concentration. G_1, S, G_2/M in each micrograph represent the percentage of cells present in normal phases of cell cycle, $SubG_1$ represents percentage of cells that undergone apoptosis/necrosis. Each histogram in panel II represents mean ± S.D. values of different phases of cell cycle obtained from all animals (n = 5) treated with varying concentrations of phorate. Control: represents the solvent control (DMSO 0.8%); *p < 0.01 as compared to control using one-way ANOVA (Dunnett multiple comparison test).

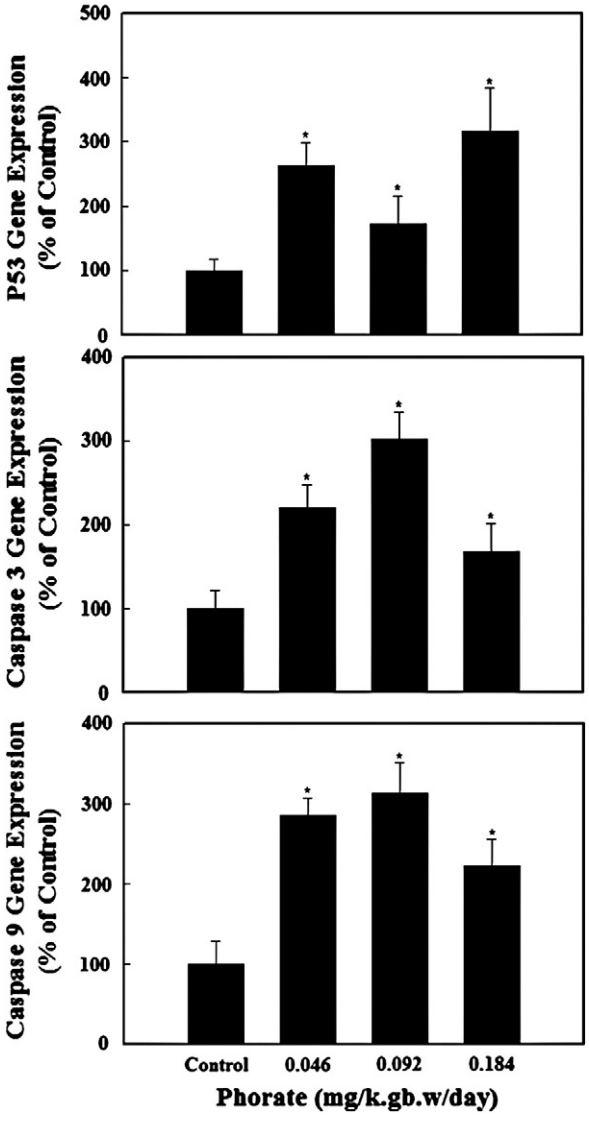

Fig. 8. Differential expression of intrinsic apoptotic pathway genes in phorate treated rats. Transcript levels were determined by real-time quantitative PCR. *$p<0.05$ using one-way ANOVA (Dunnett multiple comparison test) significantly different when compared to solvent control.

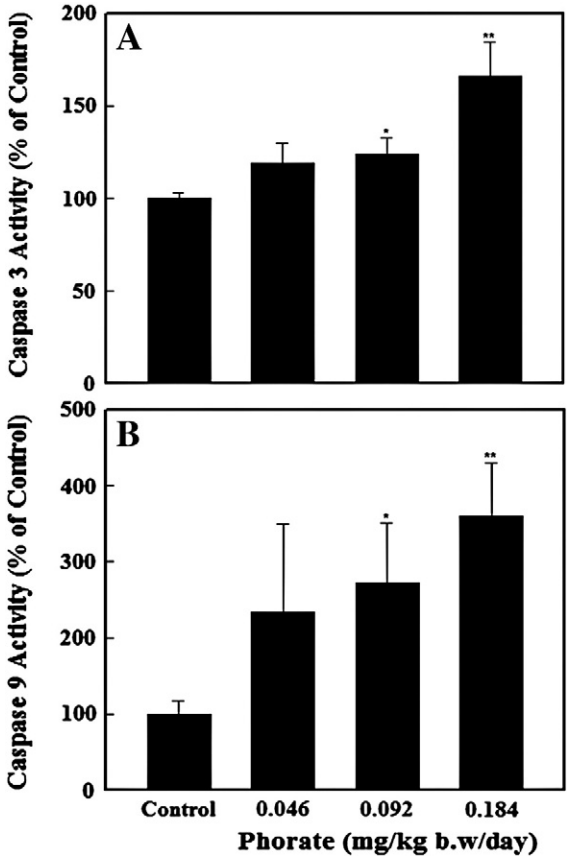

Fig. 9. Effect of phorate treatment on caspase 3 (panel A) and 9 (panel B) activities in rat liver tissue after 14 days exposure. Values are expressed as mean ± S.D. of five animals in each group. (*$p<0.05$ and **$p<0.01$) indicate significant difference from control.

oxidative stress in toxicity of phorate. The Rh123 probe accumulates electrophoretically in the strongly negative charged matrix of mitochondria in control cells, but accumulates less in mitochondria exposed to phorate. The lesser fluorescence intensity of $\Delta\Psi m$ is also consistent with perturbation of inner mitochondrial membranes, and consequent mitochondrial dysfunction as a result of ROS. Functional alterations of mitochondria are usually manifested as changes in $\Delta\Psi m$. Changes in the mitochondrial inner membrane function are accompanied by increase in outer membrane permeability, which results in release of apoptogenic factors. The effects of phorate on activation of genes related to apoptosis (p53, caspase 3 and 9) are consistent with this overall mechanism of toxic action of ROS. Typically, p53 is activated when DNA damage occurs or cells are stressed and p53 is translocated to the nucleus, where it can induce pro-apoptotic gene expression, on the mitochondrial membrane and activate the effector caspases and accelerate cell death (Levine, 1997; Sheikh and Fornace, 2000).

In general, the caspases are crucial for the activation and execution of apoptosis. The main intrinsic pathway is characterized by mitochondrial dysfunction, with the release of cytochrome c, activation of caspase 9, and subsequently of caspase 3 (Porter and Jänicke, 1999). In order to ascertain the role of phorate-induced activation of the caspase pathways, activities of caspase 9 and 3 in rat liver were measured. It is known that the extrinsic pathway is activated at the cell surface through death receptor mediated activation of caspase 8 or caspase 10, followed by caspase 3 activation. This pathway can be amplified by activation of caspase 9. Therefore, caspase 9 is regarded as one of the main initiator and caspase 3 as an effector caspase (http://www.sgul.ac.uk/depts/immunology/~dash/apoptosis/caspases.htm). Moreover, activation of caspase 3 is considered to be the "point-of-no-return" in the apoptotic signaling cascade (Green and Amarante-Mendes, 1998). In this relation, our data demonstrate significantly greater activities of caspases 3 and 9 in rats exposed to phorate, which reaffirmed their role in apoptotic pathway. Earlier studies of pesticides and organic pollutants also demonstrated activation of caspases 9 and 3 (Jin et al., 2011; Kijima et al., 2004; You and Bartolucci, 2004), and their role in inducing apoptosis, which corroborated our results. The qPCR gene expression data of caspases 9 and 3, and p53 did not exhibit a concentration-dependent response. However, activities of caspases 9 and 3 determined by ELISA demonstrated significant concentration-dependent expression of these apoptotic markers. The reason for greater activities and lesser expression of corresponding mRNAs could not be elucidated from our results. However, it might be attributed to greater post-transcriptional degradation of mRNA at a concentration of 0.184 mg/kg bw/day in case of caspase 3 and 9 genes, and 0.092 mg/kg bw/day in case of p53 gene. Such ambiguities in expression have been addressed by Merrick and Madenspacher (2005) and Korashy and El-Kadi (2004), who suggested that the plausible reason for such type of changes in specific gene expression could be differences in RNA splicing, RNA turnover, and pre and post-transcriptional modifications.

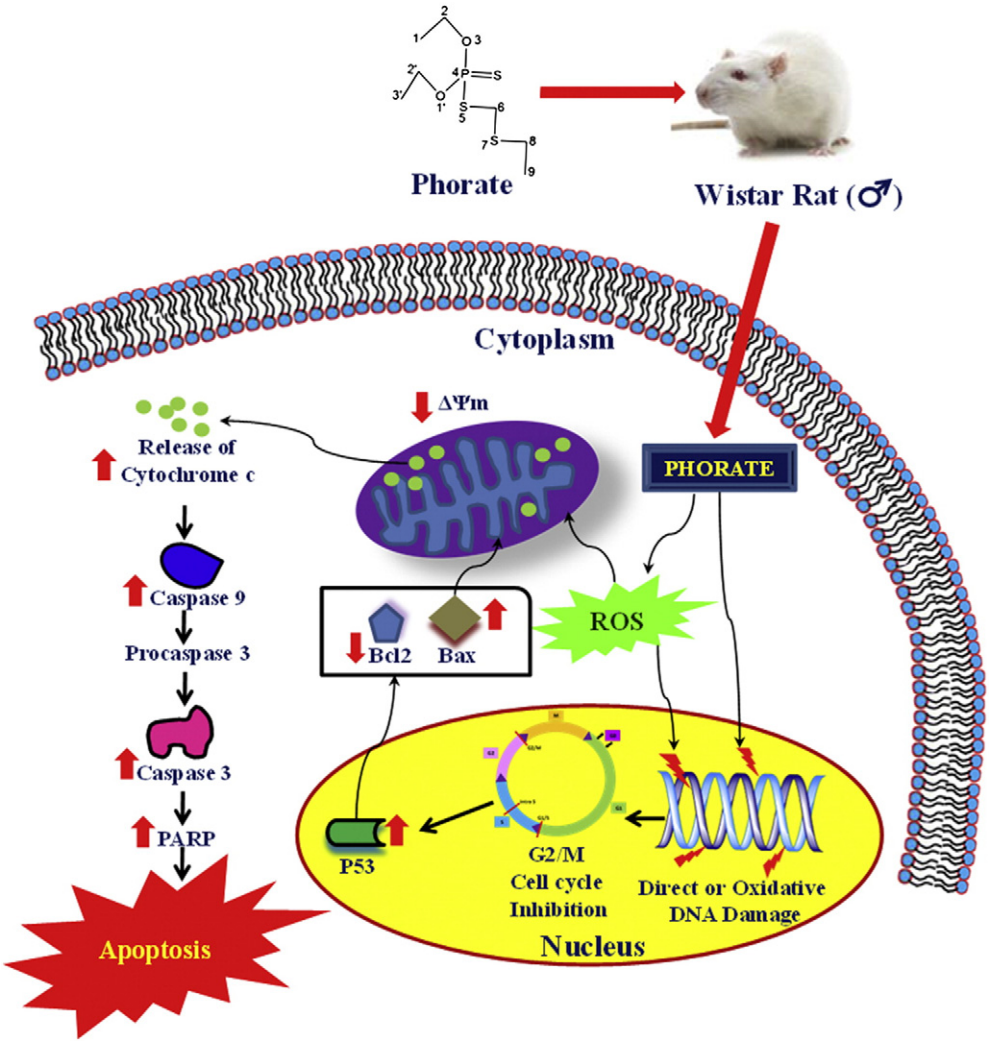

Scheme 1. Plausible mechanism of phorate-induced cellular oxidative stress and DNA damage triggering intrinsic apoptotic pathway in male Wistar rats. (↑) and (↓) arrows indicate increase and decrease in the expression of genes.

The significantly greater ($p<0.05$) OTM and comet tail length observed in bone marrow cells of rats exposed to 0.092 or 0.184 mg phorate/kg bw/day is indicative of damage to DNA. The observed DNA damage is possibly due to direct interactions of phorate or its metabolites with cellular DNA due to ROS generation causing strand breaks in DNA. The in vivo results are consistent with our previous findings in which phorate generated ROS that resulted in less $\Delta\Psi m$, which facilitates cellular damage in cultured human amnion (WISH) cells (Saquib et al., 2011). Also, the rats treated with phorate for 14 days showed G_2/M cell cycle arrest at 0.046 and 0.092 mg phorate/kg bw/day, which suggested that the DNA repair process is activated and engaged in repairing the damaged DNA by arresting the cells in G_2/M phase. However, the repair system was insufficient to repair the greater damage to DNA caused by exposure to 0.184 mg phorate/kg bw/day. Consequently, cells underwent transition from the G_2/M phase to the apoptotic phase. This is supported by the appearance of a ($SubG_1$) peak characteristic of apoptosis. Extensive DNA damage has been shown to prolong the cell-cycle arrest and eventually induces cell death (Konopa, 1988; Tsao et al., 1992). Thus, based on available information, we have proposed Scheme 1, which elucidates a plausible mechanism of induction of cellular oxidative stress, DNA damage and activation of intrinsic apoptosis pathway upon exposure to phorate. The molecular analysis led us to conclude that phorate has a potential for inducing cellular and genetic toxicity, manifested as DNA damage, disturbances in oxidative–antioxidative balance, histopathological anomalies, $\Delta\Psi m$ dysfunction, activation of apoptosis related caspase 3 and 9 genes, and appearance of SubG1 apoptotic peak in cell cycle in treated male Wistar rats.

Supplementary materials related to this article can be found online at doi:10.1016/j.taap.2011.12.006.

Funding

Financial support for this study through the Al-Jeraisy Chair for DNA Research, Department of Zoology, College of Science and the Research Center of Pharmacy, King Saud University, Riyadh, Saudi Arabia is acknowledged.

Conflict of interest

The authors declare that there is no conflict of interest.

Acknowledgments

Authors are thankful to Mr. Amin Al-Doss, Department of Zoology, King Saud University, for his help in histopathological analysis. Prof. Giesy was supported by the Canada Research Chair program, an at large Chair Professorship at the Department of Biology and Chemistry and State Key Laboratory in Marine Pollution, City University of Hong

Kong, The Einstein Professor Program of the Chinese Academy of Sciences and the Visiting Professor Program of King Saud University.

References

Abhilash, P.C., Singh, N., 2009. Pesticide use and application: an Indian scenario. J. Hazard. Mater. 165, 1–12.

Alavanja, M.C., Samanic, C., Dosemeci, M., Lubin, J., Tarone, R., Lynch, C.F., Knott, C., Thomas, K., Hoppin, J.A., Barker, J., Coble, J., Sandler, D.P., Blair, A., 2003. Use of agricultural pesticides and prostate cancer risk in the Agricultural Health study cohort. Am. J. Epidemiol. 157, 800–814.

Bagchi, D., Bagchi, M., Hassoun, E.A., Stohs, S.J., 1995. In vitro and in vivo generation of reactive oxygen species, DNA damage and lactate dehydrogenase leakage by selected pesticides. Toxicology 104, 129–140.

Bakheet, S.A., Attia, S.M., AL-Rasheed, N.M., Al-harbi, M.M., Ashour, A.E., Korashy, H.M., Abd-Allah, A.R., Saquib, Q., Al-Khedhairy, A.A., Musarrat, J., 2011. Salubrious effects of dexrazoxane against teniposide-induced DNA damage and programmed cell death in murine marrow cells. Mutagenesis 26 (4), 533–543.

Blair, A., Malker, H., Cantor, K.P., Burmeister, L., Wiklund, K., 1985. Cancer among farmers. A review. Scand. J. Work Environ. Health 11, 397–407.

Bostwick, D.G., Burke, H.B., Djakiew, D., Euling, S., Ho, S.M., Landolph, J., Morrison, H., Sonawane, B., Shifflett, T., Waters, D.J., Timms, B., 2004. Human prostate cancer risk factors. Cancer 101, 2371–2490.

Britt Jr., J.O., Martin, J.L., Okerberg, C.V., Dick Jr., E.J., 2000. Histopathologic changes in the brain, heart, and skeletal muscle of rhesus macaques, ten days after exposure to soman (an organophosphorus nerve agent). Comp. Med. 50, 133–139.

Brown, L.M., Blair, A., Gibson, R., Everett, G.D., Cantor, K.P., Schuman, L.M., Burmeister, L.F., Van Lier, S.F., Dick, F., 1990. Pesticide exposures and other agricultural risk factors for leukemia among men in Iowa and Minnesota. Cancer Res. 50, 6585–6591.

Cantor, K.P., Blair, A., Everett, G., Gibson, R., Burmeister, L.F., Brown, L.M., Schuman, L., Dick, F.R., 1992. Pesticides and other agricultural risk factors for non-Hodgkin's lymphoma among men in Iowa and Minnesota. Cancer Res. 52, 2447–2455.

Checkoway, H., DiFerdinando, G., Hulka, B.S., Mickey, D.D., 1987. Medical, life-style, and occupational risk factors for prostate cancer. Prostate 10, 79–88.

Clavel, J., Hemon, D., Mandereau, L., Delemotte, B., Severin, F., Flandrin, G., 1996. Farming, pesticide use and hairy-cell leukemia. Scand. J. Work Environ. Health 22, 285–293.

Darzynkiewicz, Z., Bruno, S., Del Bino, G., 1992. Features of apoptosis cells measured by flow cytometry. Cytometry 13, 795–808.

Devine, G.J., Furlong, M.J., 2007. Insecticide use: contexts and ecological consequences. Agric. Hum. Values 24, 281–306.

Dhingra, A.K., Grover, I.S., Adhikari, N., 1990. Chromosomal aberration and micronuclei assays of some systemic pesticides in bone marrow cells. Nucleus 33, 14–19.

Dringen, R., 2000. Metabolism and functions glutathione in brain. Prog. Neurobiol. 62, 649–671.

Fetoui, H., Garoui, E.M., Zeghal, N., 2009. Lambda-cyhalothrin-induced biochemical and histopathological changes in the liver of rats: ameliorative effect of ascorbic acid. Exp. Toxicol. Pathol. 61, 189–196.

Fulton, M.H., Key, P.B., 2001. Acetylcholinesterase inhibition in estuarine fish and invertebrates as an indicator of organophosphorus insecticide exposure and effects. Environ. Toxicol. Chem. 20, 37–45.

Gan, Q., Jans, U., 2007. Nucleophilic reaction of phorate and terbufos with reduced sulfur species under anoxic conditions. J. Agric. Food Chem. 55, 3546–3554.

Glende, E.A., Hruszkewycz, A.M., Rechnagel, R.O., 1976. Clinical role of lipid peroxidation in carbon tetra-chloride induced loss of amino pyrine demethylase, Cytochrome P450 and glucose-6-phosphatase. Biochem. Pharmacol. 25, 2163–2170.

Goel, A., Dani, V., Dhawan, D.K., 2005. Protective effects of zinc on lipid peroxidation, antioxidant enzymes and hepatic histoarchitecture in chlorpyrifos-induced toxicity. Chem. Biol. Interact. 156, 131–140.

Green, D.R., Amarante-Mendes, G.P., 1998. The point-of-no-return: mitochondria, caspases and the commitment to cell death. Cell Differ. 24, 45–61.

Gronberg, H., Damber, L., Damber, J.E., 1994. Studies of genetic factors in prostate cancer in a twin population. J. Urol. 152, 1484–1487.

Grover, I.S., Mahli, P.K., 1985. Genotoxic effects of some organophosphorus pesticides. I. Induction of micronuclei in bone marrow cells in rats. Mutat. Res. 155, 131–134.

Gupta, R.C., Singh, N., Paul, B.S., Kwatra, M.S., 1981. Role of residual estimation and clinico-biochemical and pathological changes in the diagnosis of toxicity in *Bubalus bubalis* caused by malathion. Ind. J. Anim. Sci. 51, 616–622.

Halliwell, B., Gutteridge, J.M.C., 1999. Free Radicals in Biology and Medicine, 3rd ed. Oxford Sciences Publications, Oxford.

Hassan, M.Q., Numan, I.T., A1-Nasiri, N., Stoh, S.J., 1991. Endrine-induced histopathological changes and lipid peroxidation in livers and kidneys of rats, mice, guinea pigs and hamsters. Toxicol. Pathol. 19, 108–114.

http://extoxnet.orst.edu/pips/phorate.htm (last accessed on 20.3.2011).

http://www.gezondheidsraad.nl/en/publications/health-based-reassessment-administrative-occupational-exposure-limits-phorate (last assessed on 12/4/2011).

http://www.sgul.ac.uk/depts/immunology/~dash/apoptosis/caspases.htm (last assessed on 12/8/2011).

Ivett, J.L., Myhr, B.C., 1986. Chromosomal Aberrations In Vivo in Mammalian Bone Marrow Cells on AC 35,024. Litton Bionetics, Inc, Kensington MD, USA. (LBI proj no 22202; unpublished report).

Jin, Y., Zheng, S., Pu, Y., Shu, L., Sun, L., Liu, W., Fu, Z., 2011. Cypermethrin has the potential to induce hepatic oxidative stress, DNA damage and apoptosis in adult zebrafish (*Danio rerio*). Chemosphere 82, 398–404.

Kijima, K., Toyosawa, K., Yasuba, M., Matsuoka, N., Adachi, T., Komiyama, M., Morib, C., 2004. Gene expression analysis of the rat testis after treatment with di(2-ethylhexyl) phthalate using cDNA microarray and real-time RT-PCR. Toxicol. Appl. Pharmacol. 200, 103–110.

Konopa, J., 1988. G2 block induced by DNA crosslinking agents and its possible consequence. Biochem. Pharmacol. 37, 2303–2309.

Korashy, H.M., El-Kadi, A.O.S., 2004. Differential effects of mercury, lead and copper on the constitutive and inducible expression of aryl hydrocarbon receptor (AHR)-regulated genes in cultured hepatoma Hepa 1c1c7 cells. Toxicology 201, 153–172.

Levine, A.J., 1997. p53, the cellular gatekeeper for growth and division. Cell 88, 323–331.

Lin, M.F., Wu, C.L., Wang, T.C., 1987. Pesticide clastogenicity in Chinese hamster ovary cells. Mutat. Res. 188, 241–250.

Lowry, O.H., Rosebrough, N.J., Farr, A.L., Randall, R.J., 1951. Protein measurement with Folin phenol reagent. J. Biol. Chem. 193, 265–275.

Mahajan, R., Bonner, M.R., Hoppin, J.A., Alavanja, M.C., 2006. Phorate exposure and incidence of cancer in the agricultural health study. Environ. Health Perspect. 114, 1205–1209.

Mahli, P.K., Grover, I.S., 1987. Genotoxic effects of some organophosphorus pesticides II. In vivo chromosomal aberration bioassay in bone marrow cells in rat. Mutat. Res. 188, 45–51.

Mansour, S.A., Belal, M.H., Abou-Arab, A.A.K., Gad, M.F., 2009. Monitoring of pesticides and heavy metals in cucumber fruits produced from different farming systems. Chemosphere 75, 601–609.

Merrick, B.A., Madenspacher, J.H., 2005. Complementary gene and protein studies and integrative approaches in toxicogenomics. Toxicol. Appl. Pharmacol. 207, 189–194.

Mohanty, G., Mohanty, J., Nayak, A.K., Mohanty, S., Dutta, S.K., 2011. Application of comet assay in the study of DNA damage and recovery in rohu (*Labeo rohita*) fingerlings after an exposure to phorate, an organophosphate pesticide. Ecotoxicology 20, 283–292.

Morowati, M., 1997. Inhalation toxicity studies of thimet (phorate) in Male Swiss albino mouse, *Mus musculus* I. Hepatotoxicity. Environ. Pollut. 96, 283–288.

Morowati, M., 2001. Biochemical and histopathological changes in serum creatinine and kidney induced by inhalation of thimet (phorate) in male Swiss albino mouse, *Mus musculus*. Environ. Res. 87, 31–36.

Muniz, J.F., McCauley, L., Scherer, J., Lasarev, M., Koshy, M., Kow, Y.W., Nazar-Stewart, V., Kisby, G.E., 2008. Biomarkers of oxidative stress and DNA damage in agricultural workers: a pilot study. Toxicol. Appl. Pharmacol. 227, 97–107.

Numan, I.T., Hassan, M.Q., Stohs, S.J., 1990. Endrininduced depletion of glutathion and inhibition of glutathione peroxidase activity in rats. Gen. Pharmacol. 21, 625–628.

Oruc, E.O., Usta, D., 2007. Evaluation of oxidative stress responses and neurotoxicity potential of diazinon in different tissues of *Cyprinus carpio*. Environ. Toxicol. Pharmacol. 23, 48–55.

Pagliuca, G., Serraino, A., Gazzotti, T., Zironi, E., Borsari, A., Rosmini, R., 2006. Organophosphorus pesticides residues in Italian raw milk. J. Dairy Res. 73, 1–5.

Pandita, T.K., 1986. Evaluation of Thimet 10-G for mutagenicity by 4 different genetic systems. Mutat. Res. 171, 131–138.

Porter, A.G., Jänicke, R.U., 1999. Emerging roles of caspase-3 in apoptosis. Cell Death Differ. 6, 99–104.

Saquib, Q., Al-Khedhairy, A.A., Al-Arifi, S., Dhawan, A., Musarrat, J., 2009. Assessment of methyl thiophanate-Cu (II) induced DNA damage in human lymphocytes. Toxicol. In Vitro 23, 848–854.

Saquib, Q., Al-Khedhairy, A.A., Singh, B.R., Arif, J.M., Musarrat, J., 2010a. Genotoxic fungicide methyl thiophanate as an oxidative stressor inducing 8-oxo-7,8-dihydro-2′-deoxyguanosine adducts in DNA and mutagenesis. J. Environ. Sci. Health B 45, 1–6.

Saquib, Q., Al-Khedhairy, A.A., Al-Arifi, Dutta, S., Dasgupta, S., Musarrat, J., 2010b. Methyl thiophanate as a DNA minor groove binder produces MT-Cu(II)–DNA ternary complex preferably with AT rich region for initiation of DNA damage. Int. J. Biol. Macromol. 47, 68–75.

Saquib, Q., Al-Khedhairy, Siddiqui, M.A., Roy, A.S., Dasgupta, S., Musarrat, J., 2011. Preferential binding of insecticide phorate with sub-domain IIA of human serum albumin induces protein damage and its toxicological significance. Food Chem. Toxicol. 49, 1787–1795.

Sharma-Wagner, S., Chokkalingam, A.P., Malker, H.S., Stone, B.J., McLaughlin, J.K., Hsing, A.W., 2000. Occupation and prostate cancer risk in Sweden. J. Occup. Environ. Med. 42, 517–525.

Sheikh, M.S., Fornace Jr., A.J., 2000. Role of p53 family members in apoptosis. J. Cell. Physiol. 182, 171–181.

Sobti, R.C., Krishnan, A., Pffaffenberger, C.D., 1982. Cytokinetic and cytogenetic effects of some agricultural chemicals on human lymphoid cells in vitro: Organophosphates. Mutat. Res. 102, 89–102.

Sushila, P., Alok, K.P., Mahima, B., Devendra, P., Alok, D., 2006. Cypermethrin-induced DNA damage in organs and tissues of the mouse: evidence from the comet assay. Mutat. Res. 607, 176183.

Tayeb, W., Nakbi, A., Trabelsi, M., Attia, N., Miled, A., Hammami, M., 2010. Hepatotoxicity induced by sub-acute exposure of rats to 2,4-Dichlorophenoxyacetic acid based herbicide “Désormone lourd”. J. Hazard. Mater. 180, 225–233.

Tice, R.R., Agurell, E., Anderson, D., Burlinson, B., Hartmann, A., Kobayashi, H., Miyamae, Y., Rojas, E., Ryu, J.C., Sasaki, Y.F., 2000. Single cell gel/comet assay: guidelines for in vitro and in vivo genetic toxicology testing. Environ. Mol. Mutagen. 35, 206–221.

Tsao, Y.P., D'Arpa, P., Liu, L.F., 1992. The involvement of active DNA synthesis in camptothecin-induced G2 arrest: altered regulation of p34cdc2/cyclin B. Cancer Res. 52, 1823–1829.

Van der Gulden, J.W., Vogelzang, P.F., 1996. Farmers at risk for prostate cancer. Br. J. Urol. 77, 6–14.

Van Maele-Fabry, G., Willems, J.L., 2004. Prostate cancer among pesticide applicators: a meta-analysis. Int. Arch. Occup. Environ. Health 77, 559–570.

Vandana, S., Zzaman, S., 1997. Phorate induced enzymological alterations in mouse olfactory bulb. Brain Res. Bull. 44, 247–252.
Wang, L., Liang, Y., Jiang, X., 2008. Analysis of eight organophosphorus pesticide residues in fresh vegetables retailed in agricultural product markets of Nanjing, China. Bull. Environ. Contam. Toxicol. 81, 377–382.
You, L., Bartolucci, E.J., 2004. Gene expression profiles in mammary gland of male rats treated with genistein and methoxychlor. Environ. Toxicol. Pharmacol. 18, 161–172.
Zahm, S.H., Weisenburger, D.D., Saal, R.C., Vaught, J.B., Babbitt, P.A., Blair, A., 1993. The role of agricultural pesticide use in the development of non-Hodgkin's lymphoma in women. Arch. Environ. Health 48, 353–358.